Citation: Molecular Therapy—Nucleic Acids (2015) 4, e226; doi:10.1038/mtna.2015.2

www.nature.com/mtna

Histone-targeted Polyplexes Avoid Endosomal Escape and Enter the Nucleus During Postmitotic Redistribution of ER Membranes

Nikki L Ross[1], Erik V Munsell[1], Chandran Sabanayagam[2] and Millicent O Sullivan[1]

Nonviral gene delivery is a promising therapeutic approach because of its safety and controllability, yet limited gene transfer efficacy is a common issue. Most nonviral strategies rely upon endosomal escape designs; however, endosomal escape is often uncorrelated with improved gene transfer and membranolytic structures are typically cytotoxic. Previously, we showed that histone-targeted polyplexes trafficked to the nucleus through an alternative route involving caveolae and the Golgi and endoplasmic reticulum (ER), using pathways similar to several pathogens. We hypothesized that the efficacy of these polyplexes was due to an increased utilization of native vesicular trafficking as well as regulation by histone effectors. Accordingly, using confocal microscopy and cellular fractionation, we determined that a key effect of histone-targeting was to route polyplexes away from clathrin-mediated recycling pathways by harnessing endomembrane transfer routes regulated by histone methyltransferases. An unprecedented finding was that polyplexes accumulated in Rab6-labeled Golgi/ER vesicles and ultimately shuttled directly into the nucleus during ER-mediated nuclear envelope reassembly. Specifically, super resolution microscopy and fluorescence correlation spectroscopy unequivocally indicated that the polyplexes remained associated with ER vesicles/membranes until mitosis, when they were redistributed into the nucleus. These novel findings highlight alternative mechanisms to subvert endolysosomal trafficking and harness the ER to enhance gene transfer.
Molecular Therapy—Nucleic Acids (2015) **4**, e226; doi:10.1038/mtna.2015.2; published online 10 February 2015
Subject Category: Gene vectors, Nanoparticles

Introduction

Gene transfer technologies that target dividing cells have enormous potential in biological research and therapeutics. However, although gene transfer is enhanced by cellular division,[1] low transfection efficiencies and a limited capacity to reach the nucleus necessitate improved structure/function understanding in nonviral design. Multiple works show that carrier structure influences gene transfer efficiency at least in part by determining the distribution of endocytic uptake pathways.[2] Meanwhile, a detailed understanding of structure/function relationships subsequent to endocytosis, as well as during cellular division, is necessary.

Many reports have suggested that clathrin-mediated uptake and vesicular acidification are necessary to facilitate pH-mediated release of carriers into the cytoplasm.[3] The "proton sponge effect," in which polymers with high-buffering capacity are thought to induce osmotic swelling and rupture in endosomes, is widely believed to underlie the transfection capacity of various nonviral polymers such as polyethylenimine (PEI),[4] and endosomal buffering designs remain a dominant approach in nonviral development.[3] However, multiple recent reports indicate that the endosomal buffering capacity of polymers is often uncorrelated with delivery to the nucleus or gene transfer efficiency,[5,6] and membranolytic structures face additional challenges including toxicity, limited diffusion,[7] and rapid degradation of DNA within the cytoplasm. Recent works provide insight into possible alternative trafficking patterns. For example, various studies show that the caveolar uptake route is often a more efficient gene transfer pathway for many carriers.[8,9] Native macromolecules, as well as various pathogens, are sorted within caveolae to the Golgi and endoplasmic reticulum (ER),[10] and caveolar trafficking by nanostructures is thought to reduce losses due to lysosomal degradation and promote transfer to the perinuclear region. Intriguingly, recent efforts highlight possible mechanisms to target these alternative pathways. For example, glycopolymer-based carriers were shown to exploit caveolar trafficking and colocalize significantly with the ER.[11] Additionally, our laboratory demonstrated that histone tail motifs significantly affected the trafficking of polyplexes, possibly by exploiting histone-related sorting pathways. We showed that histone 3 (H3)-derived peptides synergistically improved gene expression and greatly reduced cytotoxicity in PEI polyplexes[12] by enhancing caveolar uptake and increasing transport through the Golgi/ER.[13] A potential explanation lies in recently uncovered functions of histone methyltransferases, as a subunit within several H3 lysine 4 methyltransferases (H3K4MT)s, DPY-30, not only resides in the nucleus, but also localizes to the trans-Golgi network (TGN) and regulates retrograde transfer of cargo from endosomes.[14]

Following endocytic trafficking events, the prevailing hypothesis in dividing cells is that the majority of gene-containing vehicles enter the nucleus when the nuclear membrane breaks down during mitosis.[15,16] The correlation between enhanced cellular division and increased transfection was demonstrated by Fasbender *et al.*[1], who linked cell proliferation rate with the efficacy of lipid-based gene delivery

[1]Department of Chemical and Biomolecular Engineering, University of Delaware, Newark, Delaware, USA; [2]Delaware Biotechnology Institute, University of Delaware, Newark, Delaware, USA Correspondence: Millicent O Sullivan, Department of Chemical & Biomolecular Engineering, University of Delaware, 150 Academy St, Newark, Delaware 19716, USA. E-mail: msullivan@udel.edu
Keywords: caveolar trafficking; histone polypex; nonviral gene delovery; Rab protein
Received 12 September 2014; accepted 31 December 2014; published online 10 February 2015. doi:10.1038/mtna.2015.2

vehicles, and subsequently, similar effects have been noted in multiple other works.[15,17] While cell proliferation clearly enhances transfection, what occurs to allow endocytosed carriers to access the mitotic nucleus is less certain. The presumption that carriers partition nonspecifically from the cytoplasm into the nucleus during M-phase is inconsistent with the behavior of native proteins, which are actively transported through the nuclear pore complex based on recognition of nuclear localization signals (NLS)s. For example, the tail sequences of histones contain NLSs that interact with importin proteins to induce nuclear translocation in a cell-cycle-dependent manner.[18] Work from our laboratory as well as other reports recently showed that NLS-mediated sorting processes can greatly enhance postmitotic nuclear retention of both cytoplasmically microinjected plasmids[19] and H3 NLS-linked polyplexes.[20]

In this study, we tested the hypothesis that the altered transport and increased gene transfer efficacy of H3-targeted polyplexes was due to an increased utilization of native retrograde sorting processes as well as H3 NLS-mediated nuclear partitioning during mitosis. We detailed the trafficking behavior and pre- and postmitotic distributions of H3-targeted polyplexes in synchronized Chinese hamster ovary (CHO) cells and NIH/3T3 fibroblasts, which were previously shown to exhibit enhanced transfection by H3-targeted polyplexes.[12] We dissected specific transfer pathways associated with retrograde transport versus endosomal escape by using pulse-chase transfections and detailed imaging approaches to analyze the rate, sequence, and extent of polyplex colocalization with green fluorescent protein (GFP)-fused Rab GTPases, key regulators of cellular transport.[21] Additionally, we directly evaluated the role of endosomal escape by quantifying the kinetics of radiolabeled polyplex accumulation within the cytoplasm, and by using fluorescence correlation spectroscopy (FCS) to identify postmitotic changes in the intracellular diffusive patterns of polyplexes. Collectively, these data show that H3 targeting enhanced polyplex trafficking to the Golgi/ER *via* a stepwise vesicular pathway that may overlap with H3K4MT-linked pathways and was regulated in part by Rab6, a marker of retrograde trafficking from the Golgi to the ER. H3-targeted polyplexes were not released into the cytoplasm, but instead entered the nucleus in association with ER membranes, with a striking postmitotic increase in nuclear localization that was coincident with nuclear envelope (NE) reassembly. These studies provide valuable information on vesicular trafficking and nuclear access by nanostructures, and lend new insight on strategies to guide nonviral vehicle design.

Results

H3-targeted polyplexes traffic through Rab GTPase-linked vesicular pathways

One of the major classes of proteins regulating transfer of cargo between endomembrane organelles is the Rab family of small GTPases.[21] Rab proteins are well-known biomarkers because they have compartment-specific localization profiles and interact with key effectors that define the molecular identity of the organelles to which they are bound.[22] Because CHO cells are a routinely used model to analyze the functions of Rab-GTPases,[23] we pretransfected CHO-K1 cells with constructs encoding Rab-GFP fusion proteins to enable live visualization of polyplex colocalization dynamics.[24] To determine the extent and kinetics of H3-targeted polyplex trafficking through endolysosomal pathways, traditionally associated with proton sponge theories, versus retrograde pathways that traffic to the Golgi and/or ER, we used a pulse-chase approach to expose cells to AlexaFluor555-labeled H3-targeted polyplexes and quantified polyplex colocalization with various Rab-GFPs as a function of time by using the Manders' correlation coefficient (M_r) (**Figure 1**). Overall, Rab staining was punctate, with organelle-specific distributions consistent with the literature (**Figure 1a–e**). The polyplexes also maintained a punctate distribution and colocalized significantly with multiple Rab-linked endomembrane compartments, indicating active transport *via* various pathways including endolysosomal, recycling, and retrograde trafficking routes (**Figure 1f**).

Rab5 mediates endocytosis and early endosome fusion and is considered to be the first Rab GTPase encountered during both clathrin-mediated and caveolar endocytosis.[25] We observed an initial increase in colocalization of H3-targeted polyplexes with Rab5 and a subsequent decrease at 1-hour posttransfection. This brief transient occupancy indicated that polyplexes were rapidly transferred from Rab5-labeled compartments to other endocytic vesicles. The high overall levels of colocalization with Rab5 demonstrated that a significant fraction of polyplexes was endocytosed by clathrin-linked or caveolar vesicles, consistent with our previous studies.[13]

Rab5 cargo can transition to Rab7-late endosomal compartments, Rab9-TGN vesicles, and Rab11-recycling vesicles. Rab7 is essential for the maturation of late endosomes and fusion with the lysosomes[26]; therefore, we utilized this protein as a type of lysosomal marker. Meanwhile, Rab9 mediates transport between late endosomes and the TGN and also functions as the general organizer of late endosome subdomains.[27] Polyplex colocalization with Rab7 was slower than that observed for Rab5, consistent with literature documenting nanostructure transfer kinetics between Rab5- and Rab7-labeled structures.[22] Because Rab7 vesicles transfer some cargo to recycling vesicles instead of lysosomes,[28] we also examined polyplex colocalization with Rab11, which is associated with endocytic recycling downstream of clathrin-mediated endocytosis.[29] A portion of the H3-targeted polyplexes colocalized with Rab11 with a slightly later colocalization maximum than Rab7, suggesting that some polyplexes were indeed transported back to the plasma membrane *via* late endosomes. Meanwhile, the onset of polyplex colocalization with Rab9 also was delayed as compared with Rab5. The levels of colocalization with Rab9 remained steady until ~2 hours posttransfection, at which point the levels sharply decreased. The increase in colocalization of polyplexes with this marker, coincident with a decline in colocalization with Rab5, suggested that some polyplexes were sequentially passaged from early endosomes to TGN-sorting compartments.

To determine the mechanism of retrograde trafficking, we examined polyplex colocalization with Rab6, which regulates a native transport pathway from the Golgi to the ER[30] that is co-opted by pathogens including Shiga toxin B-fragment

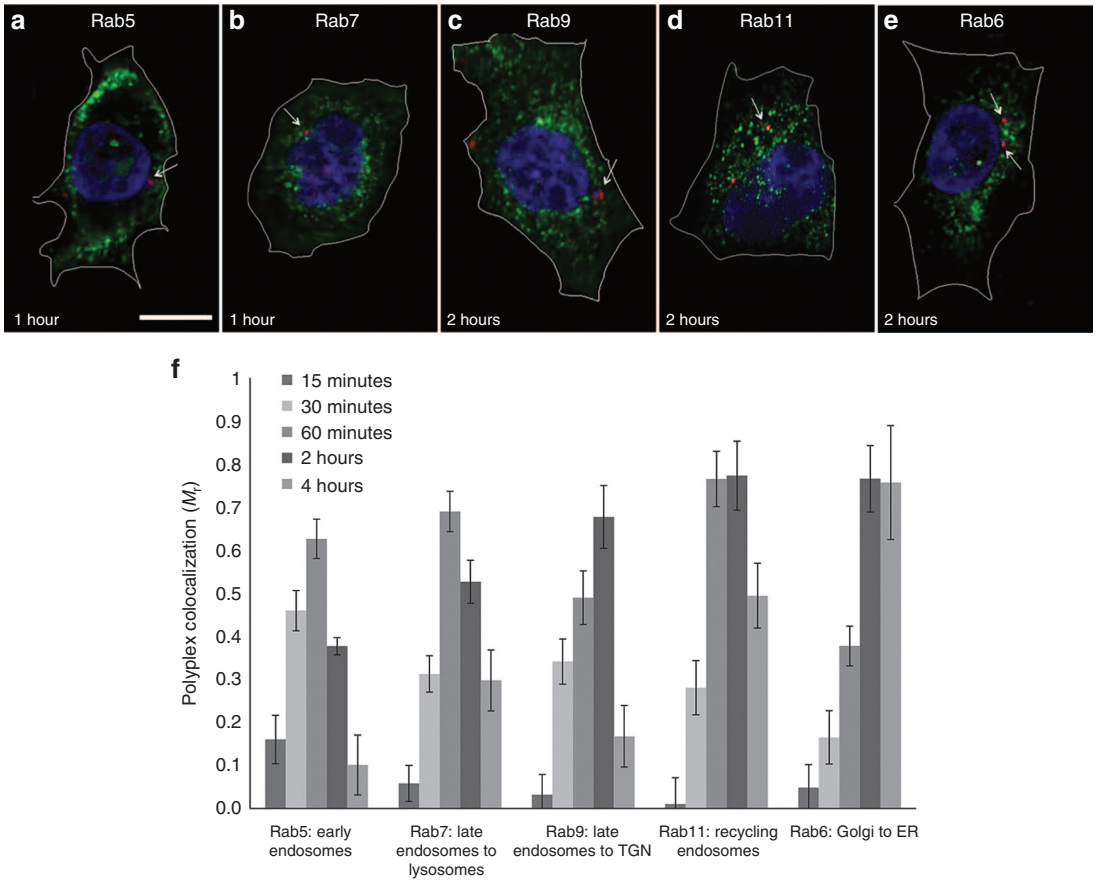

Figure 1 Colocalization of fluorescently labeled pDNA polyplexes (red) with Rab-GFPs (green) in CHO cells. (**a**–**e**) Representative confocal microscopy z-slice images of cells with nuclei stained with DAPI (blue) following a pulse transfection with the H3-targeted polyplexes. The scale bar (shown in **a**) = 10 µm. Cell images after (**a**, **b**) 1 hour or (**c**–**e**) 2 hours. (**a**) Rab5; (**b**) Rab7; (**c**) Rab9; (**d**) Rab11; and (**e**) Rab6. The cell borders were outlined in white by comparison with the corresponding phase images by using Zen software. (**f**) Quantification of colocalization between polyplexes and Rab-GFPs at different times posttransfection, performed by Volocity Image Analysis software. Each data point represents the mean ± SE for a minimum of 100 polyplexes, with ~10 images analyzed per colocalization replicate. CHO cells, Chinese hamster ovary cells; DAPI, 4′,6-diamidino-2-phenylindole; ER, endoplasmic reticulum; GFP, green fluorescent protein; TGN, trans-Golgi network.

(STB) and herpes simplex virus 1.[31] Colocalization between polyplexes and Rab6 peaked at 2 hours and then plateaued, suggesting an accumulation within Golgi/ER vesicles.

H3 targeting enhances polyplex transport through Rab5- and Rab6-linked caveolar pathways

Our previous work demonstrated that enhanced caveolar uptake was a key effect of adding H3-targeting peptides to PEI polyplexes, and that those polyplexes that were internalized within caveolae ultimately reached the nucleus and were responsible for transfection.[13] Accordingly, we sought to determine the extent to which H3-mediated changes in the initial endocytic event determined subsequent polyplex trafficking. Rab-GFP-expressing cells were transfected with H3-targeted or untargeted PEI polyplexes in the presence of established endocytic inhibitors,[32] including chlorpromazine to disrupt clathrin-coated pit formation, filipin complex III to disrupt caveolar structure/function, or genistein to disrupt the phosphorylation of caveolin.

Both clathrin and caveolar vesicles are known to traffic native proteins as well as various synthetic nanostructures through early endosomes. As shown in **Figure 2a**, clathrin inhibition minimally impacted H3-targeted PEI polyplex colocalization with Rab5, whereas caveolar inhibition reduced trafficking to early endosomes during the first hour posttransfection when polyplex transit through early endosomes was maximal (**Figure 1f**). These data suggested that a large fraction of H3-targeted polyplexes trafficked through pathways exhibiting multiple similarities to those of STB, SV40 virus, and cholera toxin,[33,34] which use caveolae/lipid rafts to travel from early endosomes directly into the Golgi and ER.[35] In contrast, clathrin cargo transfer from early endosomes to late endosomes, and ultimately, to lysosomes, the TGN, or recycling vesicles.[27] Hence, we next sought to examine the effect of endocytic inhibition on polyplex localization within these downstream structures. We saw a slight decrease in H3-targeted polyplex colocalization with the late endosomal marker Rab7 in the presence of chlorpromazine (**Figure 2b**), indicating that a fraction of H3-targeted polyplexes were trafficking *via* typical clathrin-linked endolysosomal processing routes.[36] The colocalization of untargeted polyplexes with Rab7 decreased more substantially in the presence of chlorpromazine (**Figure 3a**),

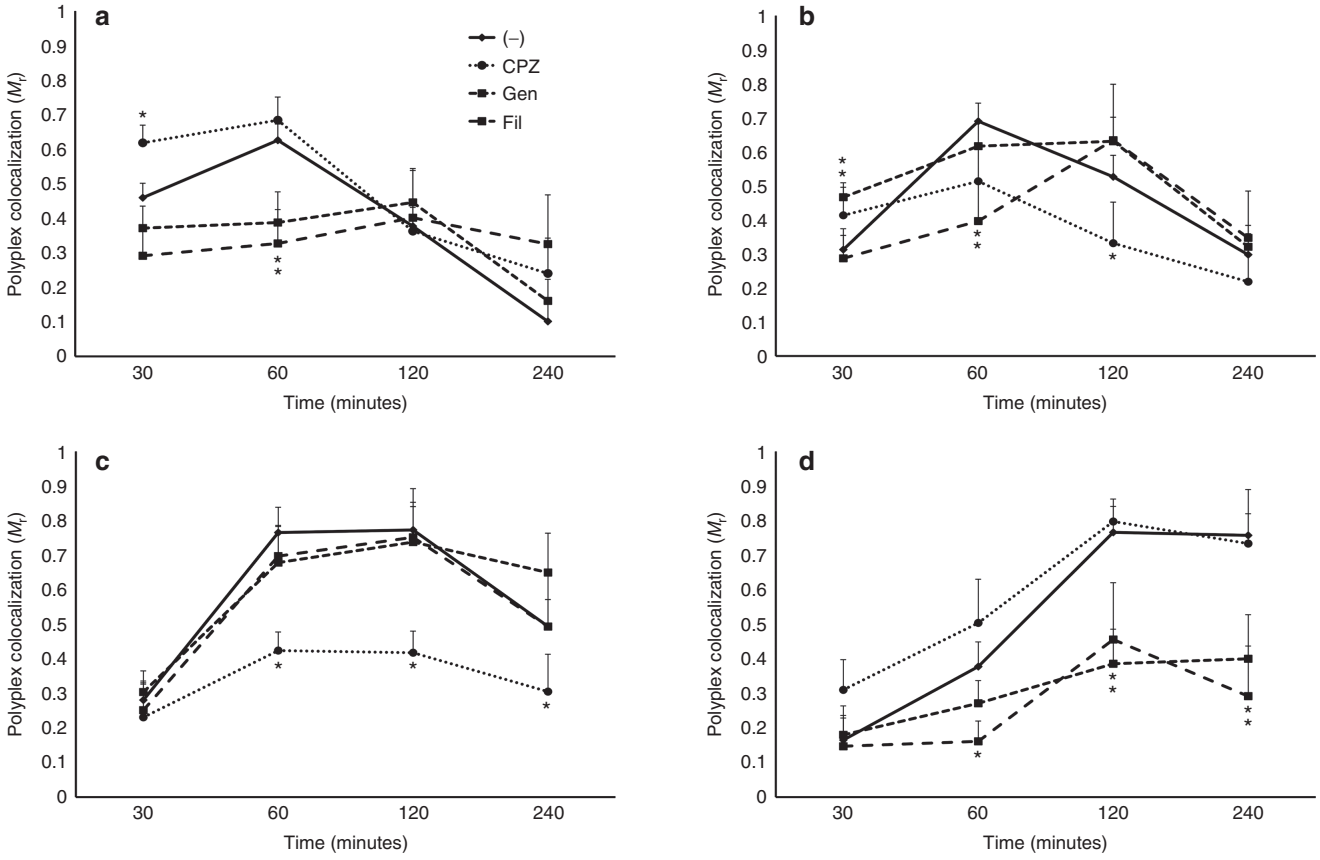

Figure 2 The effect of endocytic inhibitors on H3-targeted PEI polyplex colocalization. (**a**) Rab5; (**b**) Rab7; (**c**) Rab11; and (**d**) Rab6. Quantification of colocalization from confocal microscopy images was performed with Volocity Image Analysis software. Each sample control (–) represents colocalization values from samples in which no inhibitors were added. Each data point represents the mean ± SE in M_r values obtained by analyzing a minimum of 100 polyplexes, with ~10 images analyzed per colocalization replicate. *Indicates a statistically significant difference relative to the respective polyplex control ($P < 0.05$). CPZ, chlorpromazine; Fil, filipin complex III; Gen, genistein; PEI, polyethylenimine.

suggesting that untargeted polyplexes have an increased utilization of this pathway. The caveola e-associated inhibitors genistein and filipin complex III did not significantly change the levels of colocalization between either the targeted or untargeted polyplexes and Rab7 (**Figures 2b** and **3a**). These results agree with a previous study performed by Reilly *et al.*, in which the role of lysosomal vesicles in H3-targeted polyplex trafficking was explored by exposing cells to lysosomotropic agents during transfection. The buffering agent chloroquine had an opposite effect on the transfection efficiency of the H3-targeted polyplexes as compared with the untargeted PEI polyplexes. Specifically, chloroquine augmented the transfection efficiency for the PEI polyplexes, suggesting that a significant fraction of the PEI polyplexes trafficked through acidifying endosomes to lysosomes, and that chloroquine-mediated buffering was beneficial for the vesicular escape and transfection by these polyplexes. In contrast, the chloroquine-induced decrease in the transfection efficiencies of the H3-targeted polyplexes (~20% less than untreated controls) suggested that the H3-targeted polyplexes did not traffic to lysosomes, as buffering was not able to augment gene expression through induction of vesicular escape.

To further probe polyplex transit through downstream compartments associated with clathrin or caveolar trafficking, endocytic inhibition studies were also used to examine the effects on colocalization with the TGN marker Rab9 and the recycling vesicle marker Rab11. None of the inhibitors significantly impacted polyplex colocalization with Rab9, although minor reductions in colocalization were observed in the presence of genistein (**Supplementary Figure S1**). These results indicated that polyplexes did not reach the TGN through established clathrin-initiated routes. In contrast, H3-targeted polyplex colocalization with Rab11 was substantially reduced by endocytic inhibitors associated with clathrin but not by caveolar inhibitors (**Figure 2c**), and similar effects were observed with untargeted PEI polyplexes (**Figure 3b**). These data demonstrated that polyplex recycling occurred subsequent to clathrin-mediated uptake through a process independent of H3 targeting.

Caveolae have been reported to directly route many cargoes from the plasma membrane or early endosomes to the Golgi and/or ER,[35] and Rab6 regulates the downstream retrograde transport between early and late Golgi compartments and the ER. Hence, we next examined whether polyplexes colocalized with Rab6 downstream of caveolar uptake. In the presence of genistein or filipin complex III, there was a substantial decrease in H3-targeted polyplex/Rab6 colocalization, as shown in **Figure 2d**, suggesting that

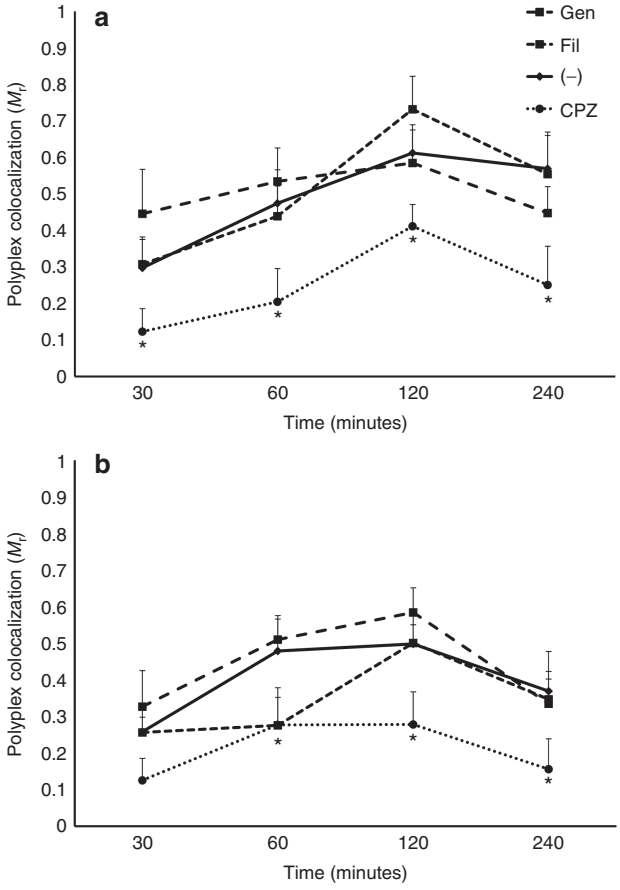

Figure 3 The effect of endocytic inhibitors on untargeted PEI polyplex colocalization. (**a**) Rab7; (**b**) Rab11. Quantification of colocalization from confocal microscopy images was performed with Volocity Image Analysis software. The respective sample control (–) was from a sample where no inhibitors were added. Each data point represents the mean ± SE for a minimum of 100 polyplexes, with ~10 images analyzed per colocalization replicate. *Indicates a statistically significant difference relative to the respective polyplex control ($P < 0.05$). CPZ, chlorpromazine; Fil, filipin complex III; Gen, genistein; PEI, polyethylenimine.

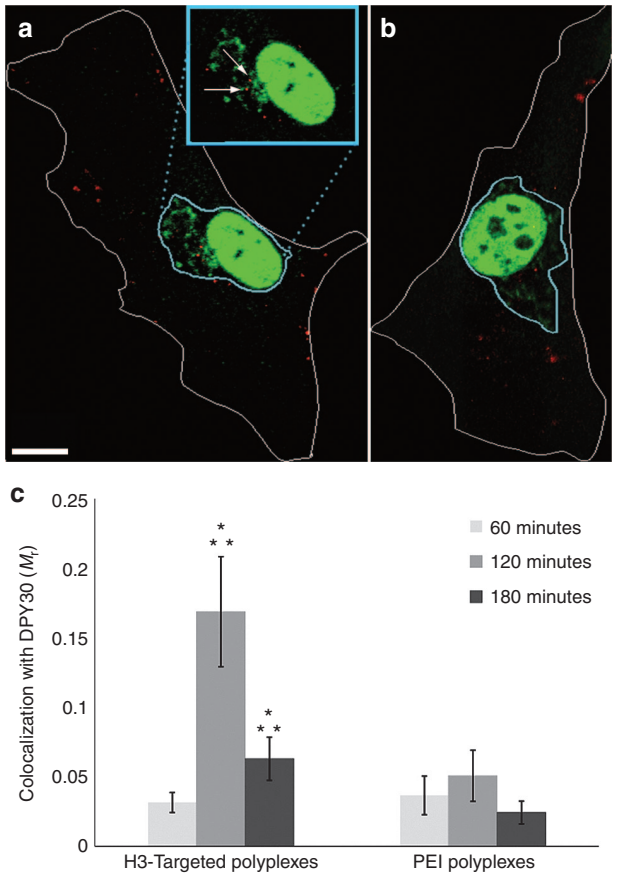

Figure 4 Colocalization of fluorescently labeled pDNA polyplexes (red) with DPY30 (green). (**a**, **b**) Representative confocal microscopy z-slice images of cells with the perinuclear regions outlined in blue. Images were taken 2 hours after a pulse transfection with (**a**) H3-targeted polyplexes or (**b**) untargeted PEI polyplexes. Scale bar (shown in **a**) = 10 µm. Cells and perinuclear regions were outlined using Zen software. Inset in **a**: Colocalization of H3-targeted polyplexes with DPY30 within the perinuclear region of the cell; arrows indicate colocalized polyplexes. (**c**) Quantification of colocalization with DPY30 from confocal microscopy images at different times posttransfection, performed by Volocity Image Analysis Software. Each data point represents the mean ± SE for a total of 20–30 cells, with a minimum of 40 polyplexes analyzed. *Indicates statistically significant difference from PEI polyplexes at the same time point ($P < 0.05$). **Indicates statistically significant difference from the previous time point for the given polyplex ($P < 0.05$). PEI, polyethylenimine.

caveolar polyplexes predominantly localized to perinuclear Rab6 structures. The effect was a function of H3 targeting, as untargeted PEI polyplexes had minimal colocalization with Rab6 ($M_r < 0.1$). Chlorpromazine had no effect on polyplex-Rab6 colocalization (**Figure 2d**).

H3 targeting increases polyplex colocalization with perinuclear mDPY-30

Recent studies have highlighted the roles of histone-processing enzymes in regulating cargo trafficking through the Golgi/ER following endocytic uptake.[14,37] Thus, we hypothesized that the H3-mediated changes in polyplex trafficking might be caused not only by the established alterations in endocytic processing, but also by interactions with mammalian DPY-30 (mDPY-30), a key subunit of H3K4MT complexes.[38] mDPY-30 localizes to both the nucleus and Golgi/ER endomembrane network, and its expression in these two regions was previously demonstrated in various mammalian cell lines including those derived from mouse, primate, and human.[14] Hence, we used pulse-chase transfections and immunostaining to quantify polyplex colocalization with mDPY-30 within the perinuclear membranes in NIH/3T3 murine fibroblasts (**Figure 4**). A fraction of the perinuclear H3-targeted polyplexes colocalized with mDPY-30, with maximal colocalization at 2 hours posttransfection (**Figure 4c**), consistent with the kinetics of enhanced H3-targeted polyplex colocalization with Rab9 (**Figure 1c**). H3-targeted polyplexes colocalized with mDPY-30 at a significantly higher level than untargeted PEI polyplexes at 2–3 hours posttransfection (**Figure 4c**), suggesting that H3 targeting increased the utilization of H3K4MT-regulated trafficking pathways.

To ensure that the altered colocalization of the H3-targeted polyplexes with H3K4MTs was sequence-specific, we also performed cellular transfection experiments with polyplexes that

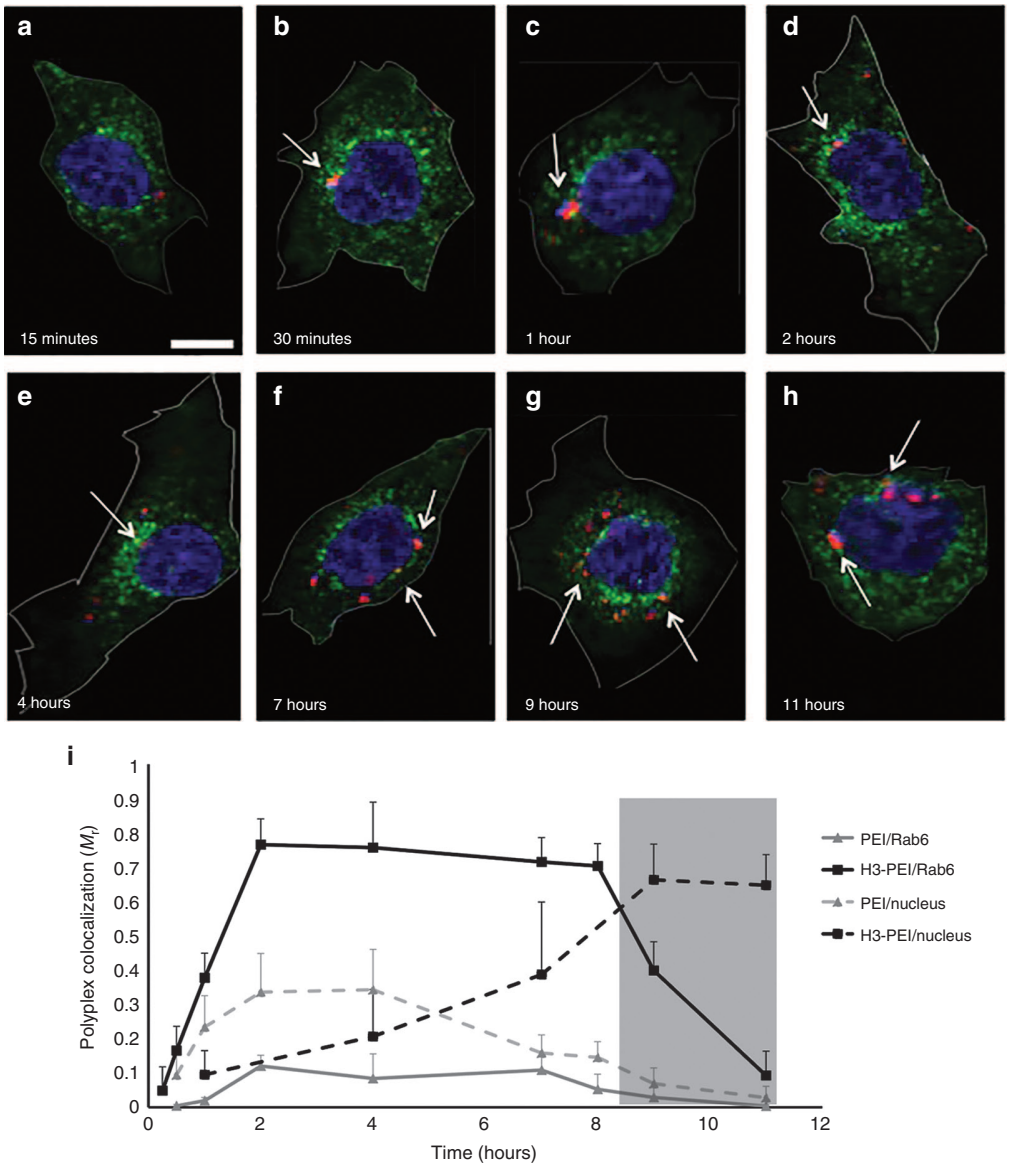

Figure 5 Colocalization of fluorescently labeled pDNA polyplexes with Rab6 at eight different time points following transfection in CHO cells. (**a-h**) Representative confocal microscopy z-slice images of cells expressing Rab6-GFP (green) with the nuclei stained with DAPI (blue) following a pulse transfection with H3-targeted PEI polyplexes (red); arrows indicate regions of colocalization between polyplexes and Rab6. The scale bar (shown in **a**) = 10 µm. The cell borders were outlined in white by comparison with the corresponding phase images by using Zen software. (**i**) Quantification of colocalization from confocal microscopy images was performed with Volocity Image Analysis software. Colocalization between H3-targeted PEI polyplexes and Rab6 (solid black) or the nucleus (dashed black); colocalization between untargeted PEI polyplexes and Rab6 (solid gray) or the nucleus (dashed gray). Each data point represents the mean ± SE for a minimum of 100 polyplexes, with ~10 images analyzed per colocalization replicate. The gray box indicates the cellular mitosis period. CHO cells, Chinese hamster ovary cells; DAPI, 4′,6-diamidino-2-phenylindole; PEI, polyethylenimine.

were assembled identically, but with a scrambled H3 sequence (sH3-targeted polyplexes) (**Supplementary Materials and Methods**). Fluorescence microscopy (**Supplementary Figure S3**) and flow cytometry analyses of GFP expression showed that only a small fraction (~10%) of cells expressed GFP when transfected with the sH3-targeted polyplexes. Additionally, pulse-chase transfections with sH3-targeted polyplexes displayed negligible cellular uptake. Therefore, the observed effects with the H3-targeted polyplexes were sequence-specific, and impacted polyplex interactions with the plasma membrane to alter endocytic trafficking.

H3-targeted polyplexes colocalize with Rab6-labeled vesicles until mitosis

While H3-targeted polyplex colocalization with most Rab-linked structures was transient following pulse transfection (**Figure 1**), the colocalization with Rab6 plateaued at 2 hours posttransfection. Because Rab6-linked cargo such as STB and other toxins ultimately translocate from the lumen of the ER to the cytosol during infection,[39] we sought to determine whether Rab6 colocalization ultimately decreased coincident with an increase in the cytosolic fraction of polyplexes. Accordingly, using synchronized CHO-K1 cells, we examined

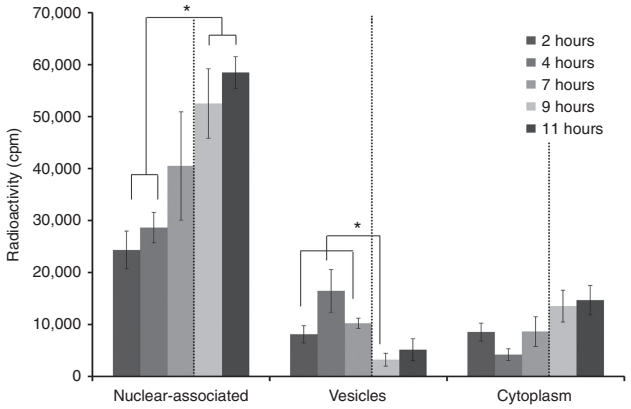

Figure 6 Intracellular distribution of [^{3}H]DNA-labeled H3-targeted PEI polyplexes in CHO cells. Cells were pulse transfected and then fractionated at the indicated time points by using differential centrifugation. Data are presented as the mean ± SE. *Indicates a statistically significant difference between the indicated samples ($P < 0.05$). The dotted line indicates the approximate time of mitosis. CHO cells, Chinese hamster ovary cells; cpm, counts per minute; PEI, polyethylenimine.

Rab6 colocalization with H3-targeted polyplexes at extended time points. Rab6 staining, as well as that of the polyplexes, remained punctate and perinuclear until mitosis (**Figure 5a–h**). During mitosis, Rab6 staining became more disperse while H3-targeted polyplex staining remained largely punctate and gradually partitioned into the nucleus. When we quantified H3-targeted polyplexes/Rab6 colocalization, we found that colocalization persisted at a high and unchanging level until division, at which time it rapidly decreased (**Figure 5i**). Untargeted PEI polyplexes exhibited little accumulation in Rab6-labeled membranes, indicating that routing through Rab6-linked vesicles was mediated by the H3 sequence.

Because of the striking decrease in H3-targeted polyplex colocalization with Rab6 during mitosis, we hypothesized that the H3-targeted polyplexes were entering the nucleus; hence, we quantified polyplex colocalization with the nuclear stain DAPI (4′,6-diamidino-2-phenylindole) over similarly extended time frames (**Figure 5i**). As compared with Rab6, an opposite effect in polyplex colocalization occurred within the nucleus, with only moderate increases in nuclear colocalization prior to mitosis and significant increases coincident with mitosis. These results suggested that premitotic accumulation in Rab6-linked compartments was necessary for H3-targeted transfection, whereas Rab6 localization and cellular division were unnecessary for nuclear colocalization by untargeted PEI polyplexes.

Cytoplasmic cellular fractions display minimal H3-targeted polyplex accumulation

As Rab6-mediated delivery into the nucleus was unexpected, we sought to confirm the apparent lack of cytoplasmic release by using plasmid radiolabeling and sucrose density gradient fractionation to quantify polyplex distribution kinetics in CHO-K1 cells. Pulse-chase transfections were used to enable kinetic detection in the isolated fractions. The vesicular fraction contained membrane-associated organelles, such as the plasma membrane, endosomes, lysosomes, Golgi, and ER. The nuclear fraction contained nucleus-associated membranes including some ER fractions.[40] A significant fraction of polyplexes localized to the nuclear fraction within 2 hours, consistent with both Rab colocalization studies (**Figure 1**) and our prior analyses involving H3-targeted polyplex colocalization with the ER marker calreticulin/KDEL.[13] Analyses of subcellular fractions indicated that the fraction of nuclear-associated polyplexes increased only moderately between 2 and 7 hours posttransfection and then significantly increased immediately following mitosis (**Figure 6**). Within the vesicle fraction, the concentration of polyplexes slowly increased from 2 to 7 hours, but then significantly decreased after mitosis. Meanwhile, the fraction of free polyplexes in the cytoplasm was small and remained unchanged during mitosis, indicating that the majority of the polyplexes were not transferred to the nucleus from the cytoplasm.

H3-targeted polyplexes enter the nucleus in slow-diffusing vesicular groupings

Recent studies indicate that the ER represents a key source of membrane for postmitotic NE reassembly, and that chromatin-mediated reshaping of the ER membranes drives NE reformation.[41] Hence, we next sought to explore whether the H3-targeted polyplexes were transported directly into the nucleus within Rab6-linked ER vesicles by analyzing the size distributions and diffusive behavior of the polyplexes during transfection. Super resolution images of transfected cells were taken at several key time points: 1 hour posttransfection; 5 hours posttransfection (*e.g.*, during the time frame of maximal Rab6 colocalization prior to mitosis); and after mitosis (24 hours posttransfection) (**Figure 7a–c**). After 1 hour, super resolution imaging identified a heterogeneous distribution of DNA-containing structures in the cytoplasm, with diameters ranging up to 2 μm (**Figure 7a**, bar graph). The smallest structures were sized similarly to free polyplexes, based on a comparison with dynamic light scattering (DLS) data.[12] Larger punctate structures of 0.4–1.7 μm were also detected, and these structures were most likely groups of polyplexes moving collectively. The quantity of the larger structures increased in the cytoplasm by 5 hours. Meanwhile, in the nucleus, few DNA-containing structures were visible prior to mitosis, but after mitosis, a population of larger structures with an average diameter of ~1 μm was visible. From these data, we can conclude that DNA entered the nucleus within multipolyplex groupings of a size similar to the size of typical endomembrane vesicles.

We next sought to use FCS to determine whether the diffusive behavior of the polyplexes during mitosis exhibited key features of an ER membrane-mediated nuclear entry mechanism, and to extract additional information on the physical properties of the polyplexes. We initially analyzed polyplexes and dyes (AlexaFluor555) in free solution to verify that these structures exhibited appropriate diffusive behavior for nanoscale assemblies versus small molecules (**Supplementary Figure S2**).[42] Subsequently, FCS data were collected in the nucleus and the cytoplasm of transfected CHO-K1 cells at time points coinciding with those of super resolution images (**Figure 7**, inset graphs). The FCS data also showed that there were two distributions of DNA-containing structures within the cytoplasm and nucleus of the cells, with one population exhibiting faster diffusive behavior similar to that of the free solution polyplexes, and the other

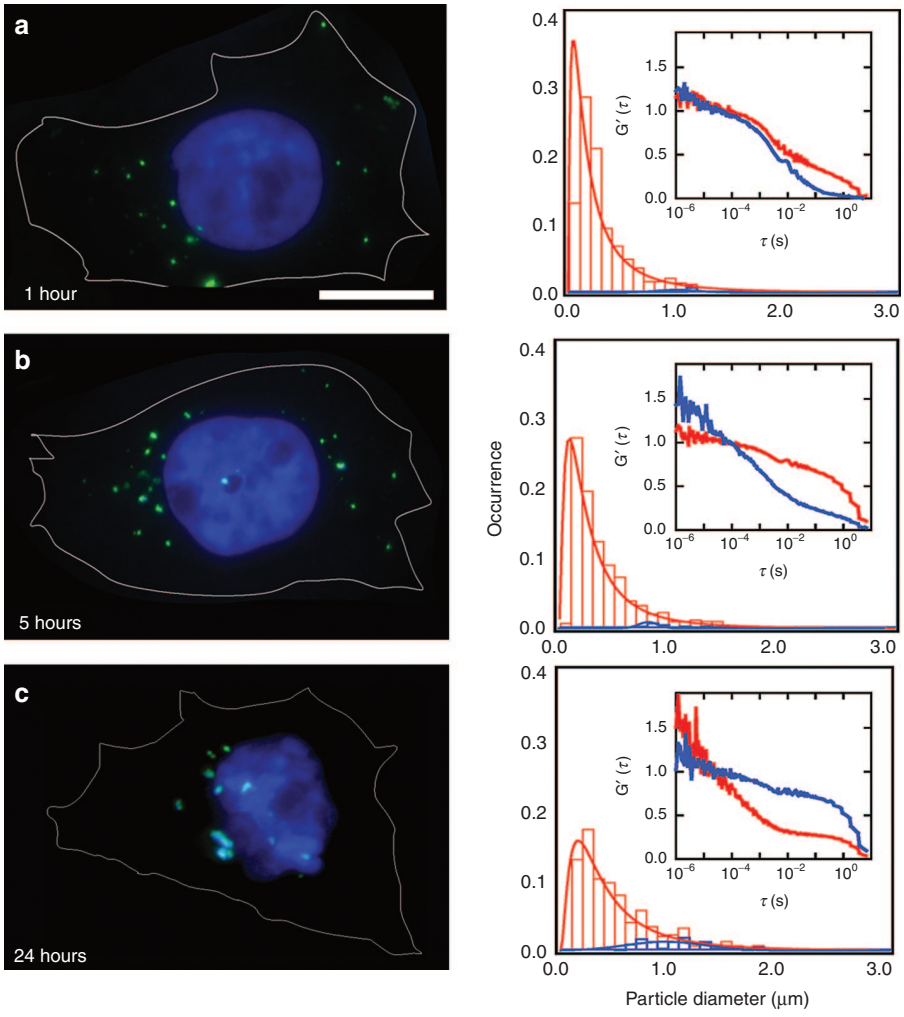

Figure 7 Super resolution microscopy and FCS analyses of transfected CHO cells at three time points posttransfection. (**a**) 1 hour; (**b**) 5 hours; and (**c**) 24 hours. Left: Representative super resolution images of polyplexes (green) within cells. The scale bar (shown in **a**) = 10 μm. The nuclei are stained with DAPI (blue). The cell borders were outlined in white by comparison with the corresponding phase images by using Zen software. Right: Histograms showing the sizes of DNA-containing structures in the nucleus (blue) and cytoplasm (red) obtained through super resolution microscopy image analysis, with normal fits indicated by lines. Ten images containing 8–10 cells per image were analyzed. Image analysis and histogram fittings were performed in ImageJ and IGOR Pro. Inset graphs: The relative intensity correlation functions, G′(τ), that were obtained through FCS analysis in the nucleus (blue) and cytoplasm (red). CHO cells, Chinese hamster ovary cells; DAPI, 4′,6-diamidino-2-phenylindole; FCS, fluorescence correlation spectroscopy.

exhibiting slower diffusive behavior (longer lag time, τ) similar to that previously reported for vesicular/membrane-bound structures.[43] The population of slow-diffusing polyplexes in the cytoplasm increased substantially by 5 hours posttransfection. At 24 hours posttransfection, the quantity of cytoplasmic polyplexes was significantly decreased. Meanwhile, a small amount of the slowly diffusing species appeared in the nucleus by 5 hours posttransfection. The fraction of this larger, slow-moving population increased after mitosis, coincident with the decrease of the slow-moving population in the cytoplasm (**Figure 7c**). These data indicated that there was a distinct postmitotic shift in the localization of the slow-diffusing population of polyplexes.

Discussion

A critical limitation of many nonviral gene delivery vehicles is their low transfection efficiency. Widely used endosomal escape approaches have variable efficacy and nanocarriers have limited diffusibility in the cytoplasm.[6,7] Additionally, although cellular mitosis can enhance gene transfer, few design criteria exist to enable maximization of this effect. Accordingly, systematic exploration of the mechanisms by which nanocarriers traverse the endomembrane network and access the nucleus are essential. Our data support an unprecedented vesicular trafficking and nuclear delivery pathway for synthetic polyplexes that parallels key aspects in the behavior of mammalian toxins, and implicates ER membrane reassembly processes in postmitotic nuclear partitioning.

PEI is the canonical proton sponge material,[4] and therefore a surprising aspect in our previous studies was that the addition of H3-targeting peptides to PEI polyplexes greatly enhanced gene transfer efficacy by routing polyplexes away from traditional endolysosomal buffering pathways that are purportedly necessary for activity.[12,13] We anticipated that the

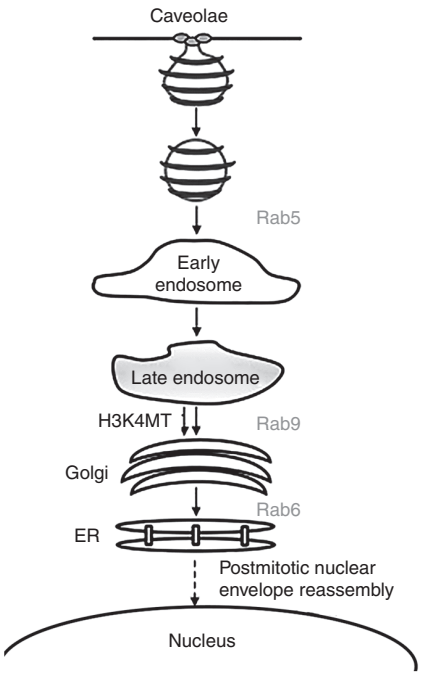

Figure 8 Proposed uptake and intracellular trafficking mechanisms for H3-targeted polyplexes. Key regulators include Rab5, Rab9/H3K4MTs, and Rab6, as well as ER membrane-mediated nuclear entry. ER, endoplasmic reticulum; H3K4MT, H3 lysine 4 methyltransferase.

H3-enhanced utilization of caveolar endocytic routes might improve activity by transferring polyplexes through compartments regulated by mDPY-30, a component in H3K4MTs that localizes to the TGN and nucleus.[14] Additionally, we sought to explore whether transfer through the Golgi/ER might more generally mimic aspects of the cellular sorting pathways used by various pathogens/toxins; the ability to localize within the ER was of great interest because many toxins translocate from the lumen of the ER to the cytosol.[44]

Colocalization studies provided evidence that both H3-targeted PEI polyplexes and untargeted PEI polyplexes were trafficked through several distinct endomembrane-linked pathways, yet not all transfer routes led to productive outcomes. Uptake through clathrin endocytosis shuttled targeted and untargeted polyplexes predominantly to Rab11-linked recycling endosomes, with a smaller fraction of polyplexes routed into Rab7-linked endolysosomal compartments (**Figures 2** and **3**). These results supported our previous studies showing that clathrin-mediated endocytosis did not lead to gene expression in H3-targeted or untargeted PEI polyplexes,[13] and that a key reason for this finding was polyplex loss *via* exocytosis. This is consistent with literature showing that clathrin-dependent uptake can also lead to polyplex recycling and impaired transfection in other types of cells.[45]

Colocalization analyses also indicated that a large fraction of the H3-targeted polyplexes, but not untargeted polyplexes, were internalized within caveolae and subsequently sorted through various retrograde pathways including those regulated by mDPY-30, as well as routes similar to those of mammalian toxins and pathogens (**Figure 8**). Approximately 18% of perinuclear H3-targeted polyplexes colocalized transiently with mDPY-30 in the TGN; these polyplexes were most likely shuttled within caveolae to the TGN *via* early endosomes, as our previous studies showed that enhanced caveolar uptake was correlated with increased transfer through Golgi-associated compartments.[13] Glycosphingolipids exhibit similar transfer patterns involving caveolar uptake followed by Rab9-dependent microtubule-mediated transport to the TGN within human skin fibroblasts.[24] However, the current study showed only a minor effect of caveolae-associated inhibitors on polyplex colocalization with Rab9 (**Supplementary Figure S1**), even though colocalization with Rab9 occurred at a high level overall. These findings may indicate that polyplex trafficking through the TGN is highly transient, consistent with the role of the Golgi apparatus in cellular sorting.

A substantial fraction of the H3-targeted polyplexes were internalized within caveolae and subsequently routed to the ER *via* pathways similar to those documented for viruses, toxins, and native cellular receptors. Indeed, many pathogens are highly efficient at exploiting normal physiological processes for their own benefit. The cellular transfer behavior of toxins like the AB toxins was of particular interest, as the AB toxins have evolved mechanisms to travel from the cell membrane to the ER/cytosol *via* early endosomes. For example, STB exploits the ER-associated protein degradation pathways to target the Golgi apparatus and ER[34] *via* a Rab6-dependent pathway, yet ultimately, STB escapes ER-associated protein degradation/proteolysis and instead retrotranslocates into the cytoplasm.[39] This process depends upon the Sec61 translocon, which was also implicated in localization of the epidermal growth factor receptor to the nucleus through a process involving retrotranslocation from the ER to the cytosol followed by importin β-mediated nuclear import.[46] Hence, the observation that H3-targeted polyplexes accumulated at high levels within Rab6-linked Golgi/ER vesicles motivated us to explore whether these polyplexes might ultimately escape the ER. However, colocalization analyses indicated that Rab6 polyplexes retained their localization until mitosis, when the distributions shifted significantly in favor of a nuclear distribution (**Figure 5i**). These results were corroborated by the data obtained from cellular fractionation studies, which showed that the levels of radiolabeled polyplexes in the cytoplasm were low and unchanging (**Figure 6**), and hence that polyplexes were most likely not transported into the nucleus from the cytoplasm. Subcellular fractionation analyses also indicated a significant decrease in the amount of vesicle-associated polyplexes and a concurrent increase in nucleus-associated polyplexes during mitosis. This suggests that H3-targeted polyplexes collected within ER-associated vesicles and were subsequently transferred into the nucleus during NE reassembly.

Cell division promotes dynamic binding and release events between membrane proteins, vesicles, and cargo,[47] and the NE also becomes increasingly permeable.[48] At the end of mitosis, recent data suggest that a key feature in NE reassembly involves the ER membrane, which can assemble around chromatin and drive NE reformation.[41] Hence, another possibility is that the H3-targeted polyplexes were directly transferred into the nucleus within Rab6-linked vesicles during ER membrane-mediated NE reassembly. Accordingly, we used super resolution imaging and FCS to determine whether

polyplexes were transferred into the nucleus in vesicle/membrane-linked groupings, as structured illumination has the ability to resolve structures as small as 50 nm, and FCS can extract the intracellular concentrations and diffusional properties of nanostructures.[43,49] Super resolution imaging indicated that intracellular polyplexes existed both individually and in larger-sized groups. The overall distribution of particle sizes did not change significantly as a function of time, but only those polyplexes that were within the larger groupings were transferred into the nucleus. FCS data were consistent with super resolution microscopy data and indicated that a slow-diffusing population of polyplexes increased in the cytoplasm between 1 hour and 5 hours, presumably reflecting the slowed mobility of the polyplexes due to collective trafficking. This population was transferred into the nucleus and out of the cytoplasm coincident with mitosis (*e.g.*, between the 5- and 24-hour time points). Comparing the FCS results to literature, the large, slowly moving population was most likely membrane-bound polyplexes within vesicles, because the correlation time was of similar order-of-magnitude as those of vesicle-entrapped objects.[43] While the fraction of the larger structures was small based on a number distribution, each one of the larger structures contained multiple polyplexes and the approximately fivefold change in diameter of the larger versus smaller structures would correlate with an ~125-fold increase in volume; hence, the slow-diffusing structures represented a significant proportion of the polyplexes. The data also suggested that this slow-diffusing population caused transfection, as gene expression did not occur until after the large-sized population reached the nucleus.

In contrast to the behavior of the H3-targeted polyplexes, untargeted polyplexes exhibited fundamentally different trafficking behavior, with earlier localization to the nucleus and a lack of dependence upon mitosis. These results are consistent with a recent study by Pun *et al.*, which found that a majority of PEI polyplexes localized to the crude nuclear fraction even at early time points (30 minutes).[40] These authors proposed that the early nuclear localization was due to incomplete separation of cytoskeletal filaments from nuclei during fractionation; hence, a portion of their polyplexes that localized to the nucleus may have in fact been cytoplasmic. In any case, the untargeted polyplexes in our study localized to the nucleus with more rapid kinetics than the targeted polyplexes, consistent with our earlier studies showing that PEI polyplexes reached the ER within minutes.[13] This difference in trafficking kinetics may indicate that the untargeted polyplexes avoid transfer through Golgi membranes and instead employ direct plasma membrane-to-ER transfer more readily than the targeted structures. It is possible that direct transfer to the ER does not provide access to the specific compartments necessary for ER-mediated transfer into the nucleus. Alternatively, the lack of an NLS in the PEI polyplexes may prevent another necessary aspect in nuclear partitioning.

Previous studies (data not included) demonstrated that the H3 peptide by itself does not enter cells and hence the altered transfection was unlikely to be caused by excess unbound peptide. Additionally, our previous experiments with untargeted PEI polyplexes clearly demonstrated that these structures on their own do not exhibit transfection activity at the same levels.[12] The significant differences in intracellular H3-targeted versus untargeted polyplex binding to histone-based enzymes, H3K4MTs (**Figure 4**), whose natural role is in engagement of the H3 tail, strongly indicated that the H3K4MTs interacted sequence-specifically with the H3-targeted polyplexes during trafficking. Additionally, the minimal cellular uptake and low transfection efficiency (**Supplementary Figure S3**) observed with sH3-targeted polyplexes demonstrated the sequence-specificity of the interactions, and indicated that the H3 sequence impacted polyplex interactions with the plasma membrane to alter endocytic trafficking.

In this study, we observed that H3 targeting enhanced polyplex transport to the nucleus by evading endolysosomal trafficking routes and harnessing retrograde pathways regulated by both histone effectors and the Rab6 GTPase. Significant new discoveries include the identification of specific mechanisms by which caveolar trafficking targets the nucleus by inducing polyplex accumulation in ER vesicles, and the finding that ER-enclosed polyplexes can efficiently enter the nucleus during postmitotic redistribution of ER membranes. These seminal findings demonstrate a need for fundamentally different approaches in nonviral design. Additionally, as gene transfer within dividing cells continues to require unreasonable excesses of DNA, improved methods to target the nucleus are essential to advance gene therapy in regenerative medicine, oncology, and a multitude of other diseases.

Materials and methods

Materials. H3 tail peptides comprised of the mammalian N-terminal H3 residues 1–25 (ARTKQTARKSTGGKAPRKQLATKAA-CONH2) were purchased from Anaspec (Fremont, CA) at ≥95% purity. The gWIZ mammalian expression plasmid encoding GFP was obtained from Genlantis (San Diego, CA), amplified in DH5α *Escherichia coli* in Lysogeny Broth, and purified with a QIAGEN Plasmid Mega Kit (QIAGEN, Valencia, CA) following the manufacturer's protocols. Prolong Gold Antifade Reagent with DAPI as well as Lipofectamine 2000 were obtained from Life Technologies (Frederick, MD). Alexa Fluor 555-labeled PNA clamps were custom-synthesized and purified to >90% by Panagene (Daejeon, Korea). Cell culture reagents were purchased from Fisher Scientific (Pittsburgh, PA). Branched PEI (25 kDa) and all other reagents were purchased at analytical grade from Sigma (St. Louis, MO). Rab-GFP plasmids were purchased from Addgene (ID#12674, 12663, 12605, 31733). Deoxycytidine-5′-triphosphate (dCTP) [5,5′-^{3}H] and Ultima Gold XR scintillation fluid were purchased from PerkinElmer (Waltham, MA). HALT protease inhibitor was obtained from Thermo Fisher Scientific (Pittsburgh, PA). Primary antibody reactive with murine DPY30 (rabbit polyclonal anti-DPY30; ab126352) was obtained from Abcam (Cambridge, MA). Secondary antibody (AlexaFluor488 anti-rabbit IgG) was obtained from Invitrogen (Carlsbad, CA).

Labeling of plasmid DNA with [3H]dCTP. Plasmid DNA (gWiz GFP) was radiolabeled with deoxycytidine 5′-triphosphate, [5-^{3}H] using a nick translation kit (GE Healthcare, Pittsburgh, PA), according to the manufacturer's instructions. G50 microspin columns (Probequant; GE Healthcare) were used to

remove unreacted nucleotides. Mass recovery was assumed to be 100%,[40] with the final labeling density of ~1×10^7 counts per minute/µg based on scintillation measurements.

Polyplex formation and transfection. For colocalization studies, pDNA was fluorescently labeled with PNA-AlexaFluor555 at a ratio of 1:20 (DNA:PNA) and H3-targeted PEI polyplexes or untargeted PEI polyplexes were formed in 20 mmol/l 4-(2-hydroxyethyl)piperazine-1-ethanesulfonic acid (HEPES) at a pH of 6 as previously described.[12] For all experiments, polyplexes were formed at an N:P ratio of 10. For polyplexes formed with a mixture of H3 and PEI, an N:P ratio of 6/4 was used where the total N:P ratio was 10, with $N = 6$ from H3 and $N = 4$ from PEI. This corresponds to ~90% (w/w) H3 and 10% PEI in the polycation solution used for pDNA complexation. For the formation of H3-targeted polyplexes, the H3 peptide was added before the PEI peptide. The amount of peptide within the polyplex was quantified previously.[50] Unless otherwise indicated, cells were pulse transfected for 15 minutes with polyplexes, and subsequently rinsed with phosphate-buffered saline (PBS) and fresh complete Dulbecco's modified Eagle's medium (DMEM) was added to the cells until a specified time point.

Cell culture and synchronization. CHO-K1 cells and mouse embryonic fibroblasts (NIH/3T3) were obtained from the American Type Culture Collection (ATCC, Manassas, VA). The cells were cultured according to ATCC protocols at 37 °C and 5% CO_2 in DMEM supplemented with 10% fetal bovine serum and 1% penicillin–streptomycin.

For CHO-K1 cell synchronization, cells were plated at ~7,200 cells/cm^2 in complete growth medium. Twenty-four hours later, lovastatin solutions in complete DMEM were added to cells at a final concentration of 10 µmol/l, and the cells were incubated for 32–36 hours. In order to resume the cell division cycle, the medium containing lovastatin was removed, the cells were washed with PBS, and fresh complete DMEM was added to cells. Cells were then incubated for an additional 12 hours so that transfection could take place during the S-phase of cell division.

For NIH/3T3 cell synchronization, cells were plated at a density of 2,000 cells/cm^2 in complete growth medium. Twenty-four hours later, the cells were washed with PBS and fresh DMEM containing 0.75% fetal bovine serum and antibiotics were added to the cells. The cells were incubated for an additional 48 hours, and then the cells were released 12 hours prior to transfection by replacing the low serum media with complete DMEM.

Rab-GFP transfection experiments. For all Rab-GFP colocalization analyses, CHO-K1 cells were plated in 8-well glass bottom plates from LabTek (Thermo Fisher Scientific, Waltham, MA), cultured for 24 hours, and synchronized. Subsequently, the cells were transfected with a specified Rab-GFP fusion plasmid in Lipofectamine for 2 hours, washed with PBS, and cultured for an additional 24 hours. Rab-GFP transfection was confirmed by fluorescence microscopy and flow cytometry to ensure that expression patterns were appropriate and that GFP was visible in a majority (~90%) of cells. Next, each well was transfected with 50 µl of polyplex solution in 150 µl of Opti-MEM containing 1 µg of pDNA labeled with PNA-AlexaFluor555. After a 15-minute "pulse" exposure to polyplexes, cells were rinsed ("chased") with PBS and then incubated in complete DMEM. At the specified time points, cells were fixed with 4% paraformaldehyde according to routine procedures.

For colocalization experiments with endocytic inhibitors, cells were treated with inhibitors both prior to as well as during transfection, according to established procedures.[13] These treatment conditions were previously optimized to minimize inhibitor-based reductions in cellular viability.

Immunocytochemistry analysis. For colocalization studies with mDPY-30, NIH/3T3 cells were plated, synchronized, and 15-minute pulse transfected with either H3-targeted polyplexes or untargeted PEI polyplexes. At the specified time points, cells were rinsed with PBS, washed with 10 µg/ml heparin, washed again with PBS, and fixed with 4% paraformaldehyde in PBS for 15 minutes. Cells were subsequently permeabilized with 0.1% saponin in PBS (Sap) and blocked with 0.5% bovine serum albumin in 0.1% Sap. A 1 µg/ml solution of primary antibody was incubated with the cells overnight at 4 °C in the blocking buffer. Cells were subsequently rinsed three times with PBS and incubated with the secondary antibody in blocking buffer for 1 hour at room temperature. Following secondary antibody treatment, cells were rinsed three more times with PBS and stored at 4 °C prior to imaging.

Confocal microscopy and quantification of polyplex colocalization. Cell imaging was performed with a 40× water immersion objective (NA = 0.55) on an LSM 5 LIVE Duo microscope (Carl Zeiss, Thornwood, NY) equipped with appropriate lasers and filters for the selected fluorescent dyes. Volocity Imaging Software (PerkinElmer) was used for image analysis and quantification of colocalization, where the locations of polyplexes and Rab proteins (or mDPY-30) were determined from measurement statistics associated with individual voxel intensities. The fraction of polyplexes (red voxels) that colocalized with the vesicle or organelle of interest (green voxels) was analyzed by calculation of the M_r, which represents the sum of the colocalized red intensity divided by the sum of the total red intensity. M_r values range from 0 (no colocalization) to 1 (complete colocalization of red voxels with green voxels).[51] Volocity software automatically determined minimum values for red and green intensities, and these minimum values were set as the threshold to distinguish signal from background. Statistical analyses of M_r values were performed using a two-tailed Student's *t*-test and the SE reported represents the population of polyplexes analyzed. A range of 40–100 polyplexes per data point in each colocalization study were analyzed to obtain these values. The number of polyplexes analyzed for each data point in each colocalization figure can be found in **Supplementary Table S1**.

Cellular fractionation and scintillation counting. For fractionation studies, polyplexes were formed with a 1:10 mixture of [^{3}H]DNA and unlabeled DNA. Cells were plated in 5 × 150 mm plates and synchronized. Subsequently, the cells were pulse transfected for 30 minutes with 10 ml of H3/PEI polyplex solution containing 200 µg of radiolabeled DNA. After the pulse

exposure, cells were washed once with PBS, replenished with complete medium, and incubated at 37 °C in 5% CO_2. To collect and fractionate cells, cells were washed twice with PBS, gently scraped off the plates with cell scrapers into 5 ml of PBS, and transferred into prechilled conical tubes. Cells were pelleted at 500*g* for 5 minutes and resuspended in 10 ml of PBS. Subsequently, cells were repelleted and then resuspended in 5 ml of homogenization buffer, comprised of 250 mmol/l sucrose, 10 mmol/l HEPES, 1 mmol/l EDTA; pH 7.4, and a 1 mmol/l protease cocktail. After centrifugation at 1,000*g* for 6 min, the resulting pellet was resuspended in homogenization buffer containing protease inhibitors. Cells were homogenized by passage through a 25-gauge needle.

After homogenization, the nuclei were pelleted at 1,000*g* for 10 minutes, separated from the postnuclear supernatant, resuspended in homogenization buffer, and pelleted a second time. The nuclear pellet was collected for analysis after the second centrifugation step, and the postnuclear supernatant from both centrifugation steps was pooled and subjected to additional fractionation procedures to separate the cytosolic and vesicle fractions. Specifically, the postnuclear supernatant was layered on top of a 10 µl cushion of 2.5 mol/l sucrose and centrifuged at 100,000*g* for 30 minutes at 4 °C in a Beckman Coulter Optima L-100 XP Ultracentrifuge (Beckman Coulter, Brea, CA). The supernatant (containing the cytosol) was transferred to a new tube, and the pellet (containing the vesicle fraction) was resuspended in 500 µl of homogenization buffer. The vesicle fraction was layered atop another 10 µl cushion of 2.5 mol/l sucrose, and the layered sample was centrifuged again at 100,000*g* for 10 minutes at 4 °C. The cytosolic supernatants were combined for analysis. After separation, all fractions were analyzed for lactate dehydrogenase activity to verify effective isolation of the cytoplasm; as anticipated, lactate dehydrogenase activity was found only in the cytoplasmic fraction (**Supplementary Figure S4** and **Supplementary Materials and Methods**).

The nuclear pellet, vesicle pellet, and cytosolic supernatant samples from fractionation studies were diluted with an equal volume of 1 mol/l NaOH to disrupt electrostatic interactions between the polymer and DNA; 4 ml of scintillation fluid was added to each sample within scintillation vials, and the vial contents were vigorously mixed. Radioactivity levels (counts per minute) were measured on a Beckman LS6000 liquid scintillation counter (Beckman Coulter, Pasadena, CA), according to routine procedures.

FCS experiments. For FCS studies, cells were plated on glass coverslips in 6-well plates and synchronized. Cells were pulse transfected for 15 minutes with polyplexes in Opti-MEM (5 µg of DNA/well), rinsed with PBS, and cultured in complete medium until a desired time point. FCS measurements were performed on an LSM 780 confocal microscope (Carl Zeiss, Oberkochen, Germany) using a 633 nm laser for excitation. The objective was a 40× (NA = 1.2) water immersion apochromat (Carl Zeiss). Samples were measured on coverslips attached to microscope slides (SecureSeals from Life Technologies) for live cell imaging. Cells were maintained at 37 °C with a stage heater. Twenty FCS readings were collected per measurement point, 10 random positions were probed per cell, and 5–10 cells were analyzed to collect the data for each sample. Autocorrelation and data analyses were performed with ZEN 2010 Software (Carl Zeiss), and 150–200 FCS curves were averaged prior to analysis. The structural parameter and measurement parameters used in analyses were determined by analyzing a standard solution of AlexaFluor555 dye in PBS and assuming a diffusion coefficient of 340 µm^2/second (**Supplementary Materials and Methods**).

Super resolution microscopy. For particle sizing *via* super resolution microscopy, CHO cells were plated in 8-well plates and synchronized. Cells were pulse transfected for 15 minutes with polyplexes in Opti-MEM (1 µg of DNA/well), rinsed with PBS, and cultured in complete medium until a desired time point. Super resolution imaging was performed on a Zeiss Elyra PS1 super resolution microscope (Carl Zeiss) using a 561 nm laser for excitation. The objective was a 63× (NA = 1.4) oil immersion apochromat (Carl Zeiss). Ten images of 75–100 cells total were analyzed to collect the data for each time point. Particle size analyses were performed using ImageJ (National Institutes of Health, Bethesda, MD). Histogram data and fits were analyzed using IGOR Pro software (WaveMetrics, Portland, OR).

Supplementary material

Figure S1. The effect of endocytic inhibitors on H3-targeted PEI polyplex colocalization with Rab9.
Figure S2. The relative intensity correlation functions.
Figure S3. Representative fluorescence microscopy images of CHO cells following transfection with H3-targeted polyplexes or scrambled H3 (sH3)-targeted polyplexes.
Figure S4. Lactate dehydrogenase activity assay to verify isolation of the cytoplasmic fraction (containing lactate dehydrogenase) during subcellular fractionation.
Table S1. The number of polyplexes analyzed for each time point in each colocalization figure.
Materials and Methods

Acknowledgments. This work was supported by the National Science Foundation under Grant No. DMR-0746458. Any opinions, findings, and conclusions or recommendations expressed in this material are those of the authors and do not necessarily reflect the views of the National Science Foundation. E.V.M. also acknowledges support provided by the National Institutes of Health Chemistry-Biology Interface Training Program under Grant No. T32GM008550. We acknowledge the Delaware Biotechnology Institute Bioimaging Facility for use of their confocal microscopes. We also thank Jeffrey L Caplan and Michael Moore for training and continuing guidance with the equipment and software used for all cellular imaging and analysis.

1. Fasbender, A, Zabner, J, Zeiher, BG and Welsh, MJ (1997). A low rate of cell proliferation and reduced DNA uptake limit cationic lipid-mediated gene transfer to primary cultures of ciliated human airway epithelia. *Gene Ther* **4**: 1173–1180.
2. Hsu, CY and Uludağ, H (2012). Cellular uptake pathways of lipid-modified cationic polymers in gene delivery to primary cells. *Biomaterials* **33**: 7834–7848.
3. Akinc, A, Thomas, M, Klibanov, AM and Langer, R (2005). Exploring polyethylenimine-mediated DNA transfection and the proton sponge hypothesis. *J Gene Med* **7**: 657–663.
4. Boussif, O, Lezoualc'h, F, Zanta, MA, Mergny, MD, Scherman, D, Demeneix, B *et al.* (1995). A versatile vector for gene and oligonucleotide transfer into cells in culture and in vivo: polyethylenimine. *Proc Natl Acad Sci USA* **92**: 7297–7301.

5. Liu, Y and Reineke, TM (2007). Poly(glycoamidoamine)s for gene delivery. structural effects on cellular internalization, buffering capacity, and gene expression. *Bioconjug Chem* **18**: 19–30.
6. Grandinetti, G, Smith, AE and Reineke, TM (2012). Membrane and nuclear permeabilization by polymeric pDNA vehicles: efficient method for gene delivery or mechanism of cytotoxicity? *Mol Pharm* **9**: 523–538.
7. Lukacs, GL, Haggie, P, Seksek, O, Lechardeur, D, Freedman, N and Verkman, AS (2000). Size-dependent DNA mobility in cytoplasm and nucleus. *J Biol Chem* **275**: 1625–1629.
8. McLendon, PM, Fichter, KM and Reineke, TM (2010). Poly(glycoamidoamine) vehicles promote pDNA uptake through multiple routes and efficient gene expression via caveolae-mediated endocytosis. *Mol Pharm* **7**: 738–750.
9. Gabrielson, NP and Pack, DW (2009). Efficient polyethylenimine-mediated gene delivery proceeds via a caveolar pathway in HeLa cells. *J Control Release* **136**: 54–61.
10. Le, PU and Nabi, IR (2003). Distinct caveolae-mediated endocytic pathways target the Golgi apparatus and the endoplasmic reticulum. *J Cell Sci* **116** (Pt 6): 1059–1071.
11. Fichter, KM, Ingle, NP, McLendon, PM and Reineke, TM (2013). Polymeric nucleic acid vehicles exploit active interorganelle trafficking mechanisms. *ACS Nano* **7**: 347–364.
12. Reilly, MJ, Larsen, JD and Sullivan, MO (2012). Histone H3 tail peptides and poly(ethylenimine) have synergistic effects for gene delivery. *Mol Pharm* **9**: 1031–1040.
13. Reilly, MJ, Larsen, JD and Sullivan, MO (2012). Polyplexes traffic through caveolae to the Golgi and endoplasmic reticulum en route to the nucleus. *Mol Pharm* **9**: 1280–1290.
14. Xu, Z, Gong, Q, Xia, B, Groves, B, Zimmermann, M, Mugler, C *et al.* (2009). A role of histone H3 lysine 4 methyltransferase components in endosomal trafficking. *J Cell Biol* **186**: 343–353.
15. Rémy-Kristensen, A, Clamme, JP, Vuilleumier, C, Kuhry, JG and Mély, Y (2001). Role of endocytosis in the transfection of L929 fibroblasts by polyethylenimine/DNA complexes. *Biochim Biophys Acta* **1514**: 21–32.
16. Brunner, S, Sauer, T, Carotta, S, Cotten, M, Saltik, M and Wagner, E (2000). Cell cycle dependence of gene transfer by lipoplex, polyplex and recombinant adenovirus. *Gene Ther* **7**: 401–407.
17. Grosse, S, Thévenot, G, Monsigny, M and Fajac, I (2006). Which mechanism for nuclear import of plasmid DNA complexed with polyethylenimine derivatives? *J Gene Med* **8**: 845–851.
18. Mosammaparast, N, Guo, Y, Shabanowitz, J, Hunt, DF and Pemberton, LF (2002). Pathways mediating the nuclear import of histones H3 and H4 in yeast. *J Biol Chem* **277**: 862–868.
19. Dean, DA, Strong, DD and Zimmer, WE (2005). Nuclear entry of nonviral vectors. *Gene Ther* **12**: 881–890.
20. Larsen, JD, Ross, NL and Sullivan, MO (2012). Requirements for the nuclear entry of polyplexes and nanoparticles during mitosis. *J Gene Med* **14**: 580–589.
21. Stenmark, H (2009). Rab GTPases as coordinators of vesicle traffic. *Nat Rev Mol Cell Biol* **10**: 513–525.
22. Sandin, P, Fitzpatrick, LW, Simpson, JC and Dawson, KA (2012). High-speed imaging of Rab family small GTPases reveals rare events in nanoparticle trafficking in living cells. *ACS Nano* **6**: 1513–1521.
23. Nayak, RC, Keshava, S, Esmon, CT, Pendurthi, UR and Rao, LV (2013). Rab GTPases regulate endothelial cell protein C receptor-mediated endocytosis and trafficking of factor VIIa. *PLoS One* **8**: e59304.
24. Choudhury, A, Dominguez, M, Puri, V, Sharma, DK, Narita, K, Wheatley, CL *et al.* (2002). Rab proteins mediate Golgi transport of caveola-internalized glycosphingolipids and correct lipid trafficking in Niemann-Pick C cells. *J Clin Invest* **109**: 1541–1550.
25. Rink, J, Ghigo, E, Kalaidzidis, Y and Zerial, M (2005). Rab conversion as a mechanism of progression from early to late endosomes. *Cell* **122**: 735–749.
26. Vanlandingham, PA and Ceresa, BP (2009). Rab7 regulates late endocytic trafficking downstream of multivesicular body biogenesis and cargo sequestration. *J Biol Chem* **284**: 12110–12124.
27. Lombardi, D, Soldati, T, Riederer, MA, Goda, Y, Zerial, M and Pfeffer, SR (1993). Rab9 functions in transport between late endosomes and the trans Golgi network. *EMBO J* **12**: 677–682.
28. Buczynski, G, Bush, J, Zhang, L, Rodriguez-Paris, J and Cardelli, J (1997). Evidence for a recycling role for Rab7 in regulating a late step in endocytosis and in retention of lysosomal enzymes in Dictyostelium discoideum. *Mol Biol Cell* **8**: 1343–1360.
29. Ullrich, O, Reinsch, S, Urbé, S, Zerial, M and Parton, RG (1996). Rab11 regulates recycling through the pericentriolar recycling endosome. *J Cell Biol* **135**: 913–924.
30. White, J, Johannes, L, Mallard, F, Girod, A, Grill, S, Reinsch, S *et al.* (1999). Rab6 coordinates a novel Golgi to ER retrograde transport pathway in live cells. *J Cell Biol* **147**: 743–760.
31. Johns, HL, Gonzalez-Lopez, C, Sayers, CL, Hollinshead, M and Elliott, G (2014). Rab6 dependent post-Golgi trafficking of HSV1 envelope proteins to sites of virus envelopment. *Traffic* **15**:157–178.
32. Ilina, P, Hyvonen, Z, Saura, M, Sandvig, K, Yliperttula, M and Ruponen, M (2012). Genetic blockage of endocytic pathways reveals differences in the intracellular processing of non-viral gene delivery systems. *J Control Release* **163**: 385–395.
33. Sandvig, K and van Deurs, B (1996). Endocytosis, intracellular transport, and cytotoxic action of Shiga toxin and ricin. *Physiol Rev* **76**: 949–966.
34. Mallard, F, Antony, C, Tenza, D, Salamero, J, Goud, B and Johannes, L (1998). Direct pathway from early/recycling endosomes to the Golgi apparatus revealed through the study of shiga toxin B-fragment transport. *J Cell Biol* **143**: 973–990.
35. Pelkmans, L, Bürli, T, Zerial, M and Helenius, A (2004). Caveolin-stabilized membrane domains as multifunctional transport and sorting devices in endocytic membrane traffic. *Cell* **118**: 767–780.
36. Vonderheit, A and Helenius, A (2005). Rab7 associates with early endosomes to mediate sorting and transport of Semliki forest virus to late endosomes. *PLoS Biol* **3**: e233.
37. Wu, CC, MacCoss, MJ, Mardones, G, Finnigan, C, Mogelsvang, S, Yates, JR 3rd *et al.* (2004). Organellar proteomics reveals Golgi arginine dimethylation. *Mol Biol Cell* **15**: 2907–2919.
38. Cho, YW, Hong, T, Hong, S, Guo, H, Yu, H, Kim, D *et al.* (2007). PTIP associates with MLL3- and MLL4-containing histone H3 lysine 4 methyltransferase complex. *J Biol Chem* **282**: 20395–20406.
39. Hazes, B and Read, RJ (1997). Accumulating evidence suggests that several AB-toxins subvert the endoplasmic reticulum-associated protein degradation pathway to enter target cells. *Biochemistry* **36**: 11051–11054.
40. Shi, J, Chou, B, Choi, JL, Ta, AL and Pun, SH (2013). Investigation of Polyethylenimine/DNA polyplex transfection to cultured cells using radiolabeling and subcellular fractionation methods. *Mol Pharm* **10**: 2145–2156.
41. Anderson, DJ and Hetzer, MW (2008). Shaping the endoplasmic reticulum into the nuclear envelope. *J Cell Sci* **121** (Pt 2): 137–142.
42. Sabanayagam, CR, Oram, M, Lakowicz, JR and Black, LW (2007). Viral DNA packaging studied by fluorescence correlation spectroscopy. *Biophys J* **93**: L17–L19.
43. Clamme, JP, Krishnamoorthy, G and Mély, Y (2003). Intracellular dynamics of the gene delivery vehicle polyethylenimine during transfection: investigation by two-photon fluorescence correlation spectroscopy. *Biochim Biophys Acta* **1617**: 52–61.
44. Sandvig, K, Garred, O, Prydz, K, Kozlov, JV, Hansen, SH and van Deurs, B (1992). Retrograde transport of endocytosed Shiga toxin to the endoplasmic reticulum. *Nature* **358**: 510–512.
45. Gonçalves, C, Mennesson, E, Fuchs, R, Gorvel, JP, Midoux, P and Pichon, C (2004). Macropinocytosis of polyplexes and recycling of plasmid via the clathrin-dependent pathway impair the transfection efficiency of human hepatocarcinoma cells. *Mol Ther* **10**: 373–385.
46. Liao, HJ and Carpenter, G (2007). Role of the Sec61 translocon in EGF receptor trafficking to the nucleus and gene expression. *Mol Biol Cell* **18**: 1064–1072.
47. Symens, N, Soenen, SJ, Rejman, J, Braeckmans, K, De Smedt, SC and Remaut, K (2012). Intracellular partitioning of cell organelles and extraneous nanoparticles during mitosis. *Adv Drug Deliv Rev* **64**: 78–94.
48. Lénárt, P and Ellenberg, J (2006). Monitoring the permeability of the nuclear envelope during the cell cycle. *Methods* **38**: 17–24.
49. DeRouchey, J, Schmidt, C, Walker, GF, Koch, C, Plank, C, Wagner, E *et al.* (2008). Monomolecular assembly of siRNA and poly(ethylene glycol)-peptide copolymers. *Biomacromolecules* **9**: 724–732.
50. Larsen, JD, Reilly, MJ and Sullivan, MO (2012). Using the epigenetic code to promote the unpackaging and transcriptional activation of DNA polyplexes for gene delivery. *Mol Pharm* **9**: 1041–1051.
51. Manders, E, Verbeek, F and Aten, J (1993). Measurement of colocalization of objects in dual-color confocal images. *J Microscopy-Oxford* **169**: 375–382.

Supplementary Information accompanies this paper on the Molecular Therapy–Nucleic Acids website (http://www.nature.com/mtna)